J|A|C|S
ARTICLES

Published on Web 02/18/2010

Reaction Pathways and Possible Path Bifurcation for the Schmidt Reaction

Tetsuji Katori, Shuhei Itoh, Makoto Sato, and Hiroshi Yamataka*

Department of Chemistry and the Research Center for Smart Molecules, Rikkyo University, Nishi-Ikebukuro, Toshima-ku 171-8501 Tokyo, Japan

Received October 25, 2009; E-mail: yamataka@rikkyo.ac.jp

Abstract: The N_2 liberation from iminodiazonium ion (**2-X**) is a key step of the Schmidt rearrangement of ketones. Molecular orbital calculations showed that two concurrent reaction channels, *syn*-benzyl fragmentation and *anti*-Me rearrangement, exist for ***syn*-2**, whereas ***anti*-2-X** proceeds via a single TS. Substituent effect analyses of the reactions of ***syn*-2-X** gave concave-upward plots, typical for a concurrent reaction mechanism. On the other hand, the reactions of ***anti*-2-X** gave linear Hammett plots, indicative of a single reaction mechanism for all ***anti*-2-X**. IRC calculations, however, revealed that the TS led to either an *anti*-benzyl rearrangement or an *anti*-benzyl fragmentation product depending on the substituent. Thus, the change of the mechanism (identity of the product) could not be detected by the Hammett plots. Ab initio dynamics simulations for ***anti*-2-X** were found to follow the IRC path for X = *p*-NO_2, giving the rearrangement product, and almost so for X = *p*-MeO, giving the fragmentation products. However, in borderline cases where X is less donating than *p*-MeO and less withdrawing than *p*-NO_2, the trajectories did not follow the minimum energy path on the potential energy surface but gave both rearrangement and fragmentation products directly from the single TS. This is a novel example of path bifurcation for a closed shell anionic reaction. It was concluded that a reactivity-selectivity argument based on the traditional TS theory might not always be applicable even to a well-known textbook organic reaction.

Introduction

The Schmidt and Beckmann rearrangements are well-known rearrangement reactions to an electron-deficient nitrogen center.[1] Both reactions give a rearranged acid amide from a ketone. However, the reaction mechanism is much less known for the Schmidt compared to the Beckmann rearrangement.

The reaction pathway is often written as eq 1, in which azidehydrin (AH) and iminodiazonium ion (ID) are important intermediates. Although there has been a claim that an amide is directly formed from AH,[2] ID is commonly considered to be the precursor intermediate for the rearrangement.[3−6] The reaction of $PhCH{=}C(CH_3)N_3$ under acidic conditions was shown to give a mixture of $PhCH_2$- and CH_3-migrated amides, the ratio of which was the same as that observed for the Schmidt reaction of $PhCH_2COCH_3$. The results indicated that ID ($PhCH_2C(CH_3)N_3^+$) was the common precursor of the two reactions.[5] The *syn*−*anti* isomerization barrier was considered to be lower in the Schmidt than Beckmann reaction.[5] Computational results at a rather low level of theory (HF/6-31G*) for the parent compound ($H_2C{=}N{-}N_2^+$) indicated that the barrier for isomerization was 14.5 kcal/mol.[7] Product analysis experiments for the Schmidt reactions of ketones ArCOR showed that the fraction of R rearrangement increased with the steric bulk of R,[3,4] which suggested that *syn*−*anti* isomerization in ID was slow, and a group that was located *anti* to N_2 migrated preferentially. The effect of substituent on the product ratio for the reactions of substituted benzophenones was reported to be small,[5] but information on the rate-determining step of the reaction is scarce. No kinetic measurement was carried out that allows one to analyze substituent effects. The ID ion, $AnCH{=}N{-}N_2^+$, was shown to undergo hydrolysis to give AnCHO in wet CH_3CN rather than to give amide via the Schmidt reaction.[6,8] In another mechanistic aspect, the Schmidt rearrangement of ketones and aldehydes is known to yield fragmentation products in addition to the expected rearrangement products, depending on the R^2 group,[6,8] in a way analogous to the Beckmann reaction of ketoximes.[9,10]

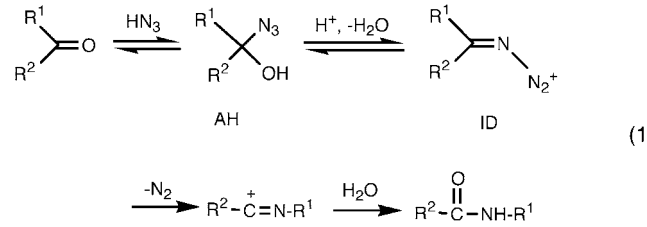

(1)

Thus, several issues still remain unsolved for the Schmidt reaction: (1) the rate-determining step of this multistep reaction, (2) relevance of *syn*−*anti* isomerization to the reaction mechanism, (3) electronic effects on the reaction rates, and (4) factors that determine the product ratio. It is difficult to address issue 1 on the basis of gas-phase calculations only, and the identifica-

(1) Smith, P. A. S. In *Molecular Rearrangements*; de Mayo, P. , Ed.; Wiley: New York, 1963; Vol. 1, Chapter 8.
(2) Fikes, L. E.; Shechter, H. *J. Org. Chem.* **1979**, *44*, 741.
(3) Szmant, H. H.; McIntosh, J. J. *J. Am. Chem. Soc.* **1950**, *72*, 4835.
(4) Smith, P. A. S.; Horwits, J. P. *J. Am. Chem. Soc.* **1950**, *72*, 3718.
(5) Hassner, A.; Ferdinandi, E. S.; Isbister, R. J. *J. Am. Chem. Soc.* **1970**, *92*, 1672.
(6) Richard, J. P.; Amyes, T. L.; Lee, Y.-G.; Jagannadham, V. *J. Am. Chem. Soc.* **1994**, *116*, 10833.

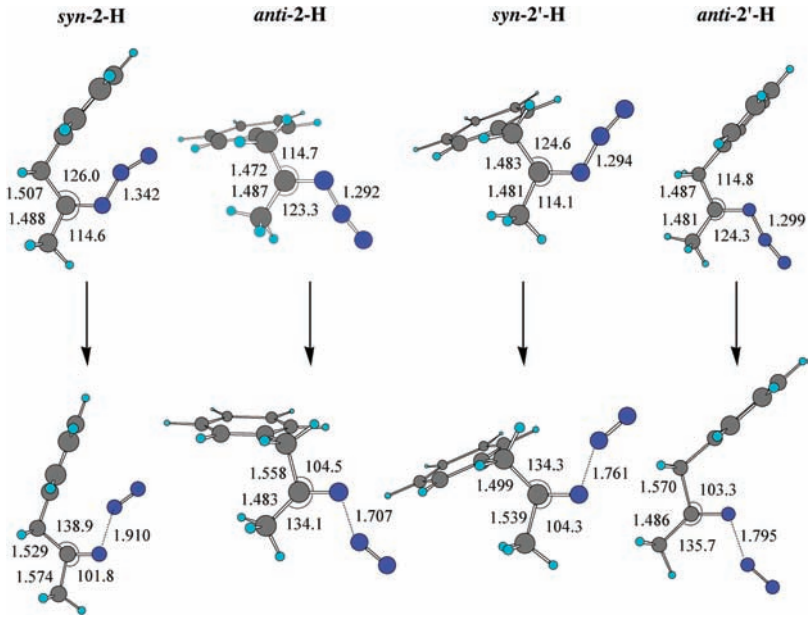

Figure 1. Optimized structures of the ID ions and their respective TSs for the Schmidt reaction at MP2/6-31G*. Atomic distances are in angstroms, and angles are in degrees.

tion requires a kinetics experiment, which would be a separate study. In the present study, we have carried out molecular orbital (MO) calculations to deal with issues 2−4. We have recently demonstrated by means of ab initio MO and molecular dynamics (MD) studies that oximes of 1-phenyl-2-propanone and 3-phenyl-2-butanone give both rearrangement and fragmentation products, depending on the substituent on the phenyl ring, and that the two types of products are formed via path bifurcation after the rate-determining transition state (TS).[10] In order to further clarify the point raised as issue 4, we have also carried out MD study for the reactions of ID ions (**2-X**) derived from 1-X-substituted phenyl-2-propanone with the aim of clarifying the reaction mechanism of the Schmidt reaction of ketones and of showing possible occurrence of dynamic path bifurcation in the reaction.

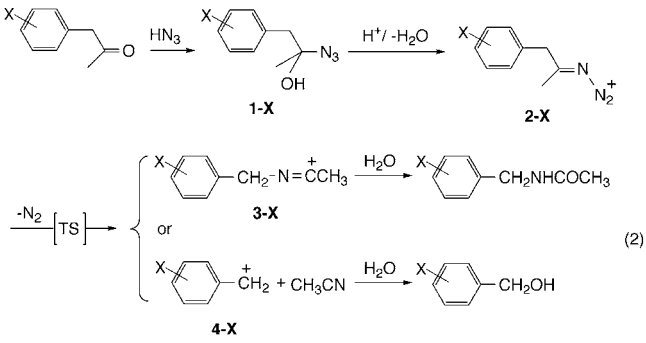

Computational Methods

Structures of **1-X** (AH), **2-X** (ID), **3-X**, **4-X**, and the TSs of the N_2-liberation step in eq 2 were fully optimized at HF/6-31G* and MP2/6-31G* for X = *p*-NH_2, *p*-MeO, *p*-OH, *m*,*p*-Me_2, *p*-Me, *m*,*m*-Me_2, *m*-Me, H, *p*-F, *p*-Cl, *m*-Cl, *p*-CHO, *p*-CN, and *p*-NO_2 by using the Gaussian 03 suite of program.[11] The TSs of the CH_2−N dissociation step of **3-X** to **4-X** were also determined for selected substrates. Energies of products are for separated species rather than product complexes. In **2-X**, *syn* and *anti* isomers were optimized, and the reactions of these isomeric species were examined. Full frequency calculations were carried out for all optimized structures to confirm whether the structures are on a minimum or a saddle point on the potential energy surface (PES). Intrinsic reaction coordinate (IRC) calculations were performed for all TSs at the HF and MP2 computational levels.

Trajectory calculations were carried out by using G03 with BOMD keyword at the HF and MP2 levels of theory.[11] Simulations were initiated at each TS for a series of substituted derivatives with quasi-classical normal mode sampling and continued up to 500 fs with average stepsize of 0.5 fs at 298 K. Trajectories either led to the product states (productive run) or went back to the reactant state (non-productive run), and only the fates of the productive runs are discussed in the paper.

Table 1. Relative Energies of the ID Ions and Their Respective TSs and Product States for **2-H**[a]

method	species	ID ion	TS	product
HF/6-31G*	***syn*-2-H**	0.0 (0.0)	2.6 (2.2)	–74.1 (–86.7)
	***anti*-2-H**	0.4 (0.0)	2.5 (1.6)	–56.8 (–79.7)
	***syn*-2′-H**	1.2 (0.7)	3.4 (2.6)	–74.1 (–86.7)
	***anti*-2′-H**	2.3 (0.6)	4.7 (3.8)	–56.8 (–79.7)
MP2/6-31G*	***syn*-2-H**	0.0 (0.0)	13.2 (12.2)	–53.7 (–67.6)
	***anti*-2-H**	5.0 (4.0)	17.0 (15.0)	–55.8 (–69.4)
	***syn*-2′-H**	5.7 (4.7)	18.6 (16.5)	–53.7 (–67.6)
	***anti*-2′-H**	7.5 (5.7)	22.1 (18.7)	–55.8 (–69.4)

[a] Calculated enthalpies (free energies) in kcal/mol.

Results and Discussion

Reaction of Parent Species. Optimization of **2-H** gave a pair of *anti* and *syn* ID forms (***syn*-2-H**, ***anti*-2-H**, ***syn*-2′-H**, and ***anti*-2′-H**), and each of the ID species gave a distinct TS upon the C−N bond cleavage. The optimized structures of these ID species and TSs are shown in Figure 1, and the relative energies of the IDs, TSs, and the reaction intermediates are listed in Table 1.

It is interesting to see in Table 1 that ***syn*-2-H** is the most stable form both at ID and TS. The stability of the *syn* form likely arises from an interaction between the π-system of the phenyl ring and the positively charged central nitrogen atom of N_3. The IRC from the TS of ***syn*-2-H** leads to migration of the

(7) Bach, R. D.; Wolber, G. J. *J. Org. Chem.* **1982**, *47*, 239.
(8) Amyes, T. L.; Richard, J. P. *J. Am. Chem. Soc.* **1991**, *113*, 1867.

Table 2. Calculated Activation Energies and Selected TS Geometrical Parameters at MP2/6-31G* for the Reactions of ***syn*-2-X**

X	activation energies[a]	reaction energies[b]	R_{Bn-C}[c]	R_{C-Me}[d]	R_{N-N2}[e]	θ_{Me-C-N}[f]
p-NH_2	7.7 (7.1)	–40.9 (–65.2)	1.630	1.516	1.842	123.8
p-OMe	10.8 (9.9)	–35.6 (–60.0)	1.653	1.521	1.874	124.2
p-OH	11.7 (10.8)	–33.8 (–58.0)	1.655	1.524	1.882	123.8
m,*p*-Me_2	13.3 (12.1)	–29.3 (–53.6)	1.656	1.531	1.910	122.4
p-Me	13.4 (12.2)	–28.5 (–52.7)	1.650	1.534	1.921	121.4
m,*m*-Me_2	14.0 (12.6)	–52.0 (–66.2)	1.534	1.577	1.938	102.0
m-Me	13.6 (12.4)	–52.9 (–66.7)	1.532	1.576	1.924	101.9
H	13.2 (12.2)	–53.7 (–67.6)	1.529	1.574	1.910	101.8
p-F	13.3 (12.2)	–53.6 (–67.3)	1.533	1.574	1.916	102.4
p-Cl	13.3 (12.2)	–53.7 (–67.4)	1.530	1.573	1.911	102.2
m-Cl	13.2 (12.4)	–54.4 (–67.9)	1.523	1.571	1.890	101.4
p-CHO	13.1 (12.3)	–54.7 (–68.1)	1.523	1.570	1.886	101.5
p-CN	13.0 (12.3)	–55.3 (–68.5)	1.521	1.569	1.875	101.5
p-NO_2	13.0 (12.5)	–55.7 (–68.7)	1.518	1.567	1.862	101.3

[a] $\Delta H^{\ddagger}$ ($\Delta G^{\ddagger}$) in kcal/mol with respect to ***syn*-2-X**. [b] ΔH (ΔG) in kcal/mol with respect to ***syn*-2-X**. Reaction energies are for the $PhCH_2$-fragmentation products for X = *p*-NH_2−*p*-Me, and for the Me-rearrangement products for X = *m*,*m*-Me_2−*p*-NO_2. [c] Distance between benzylic carbon and imino carbon in Å. [d] Distance between Me carbon and imino carbon in Å. [e] Distance between imino N and N_2 in Å. [f] Angle of methyl carbon and C=N in deg.

methyl group, which is located *anti* to the leaving group, N_2. The second stable isomer of **2-H** is ***anti*-2-H**, whose TS leads to the benzyl rearranged product as expected.

Barriers of interconversion among the four isomeric IDs were calculated at MP2/6-31G*. The two *syn* isomers, ***syn*-2-H** and ***syn*-2′-H**, were connected though the C−CH_2Ph bond rotational TS, which is 8.2 (8.9) kcal/mol higher in enthalpy (free energy) than ***syn*-2-H**. Similarly, ***anti*-2-H** and ***anti*-2′-H** isomers will interconvert through a C−CH_2Ph bond rotational TS, which is 7.7 (8.0) kcal/mol unstable compared to the ***syn*-2-H** isomer. Interconversion between ***syn*-2′-H** and ***anti*-2-H** and between ***syn*-2-H** and ***anti*-2′-H** occurs through the isomerization at the C=N bond. Such isomerization may occur via a rotational mechanism at the C=N bond, in which the $PhCH_2$−C=N−N_2 dihedral angle would be the main reaction coordinate, or via an inversion mechanism, in which the C=N−N_2 angle is the reaction coordinate. The rotational mechanism is normally preferred for a compound with a weak C=N bond, whereas the inversion mechanism operates for a compound whose TS is stabilized by a conjugation between a group on the N terminal and the C=N double bond or the lone-pair electrons on N.[12] For the present system, only rotational TSs could be optimized, and the relative energies of the TSs with respect to ***syn*-2-H** were 23.4 (24.8) kcal/mol for the ***syn*-2′-H**/***anti*-2-H** isomerization and 31.5 (29.7) kcal/mol for the ***syn*-2-H**/***anti*-2′-H** isomerization. These *syn*/*anti* isomerization TSs are much higher in energy than the TSs for the Schmidt reactions of ***syn*-2-H** and ***anti*-2-H** as described below, and therefore the Schmidt reactions of ***syn*-2-H** and ***anti*-2-H** can be treated as independent reactions. In the following discussion, we will concentrate on the results for the reactions of these *syn* and *anti* forms at the MP2 level.

Reactions of *syn*-2-X. The structures of TSs for the reactions of ***syn*-2-X** were fully optimized, and the activation energies and selected geometrical parameters are listed in Table 2. It can be seen in Table 2 that there is clear discontinuity in the geometrical parameters between the *p*-Me and *m*,*m*-Me_2 TSs. The results appear to suggest that the nature of the TS and the reaction mechanism are different for ***syn*-2-X** with a more electron-donating substituent than *p*-Me and for ***syn*-2-X** with a less electron-donating substituent than *m*,*m*-Me_2 or with an electron-withdrawing substituent. The IRC calculations indicated that the two sets of substrates indeed gave different products. Typical examples are shown in Figure 2. It is clear that the

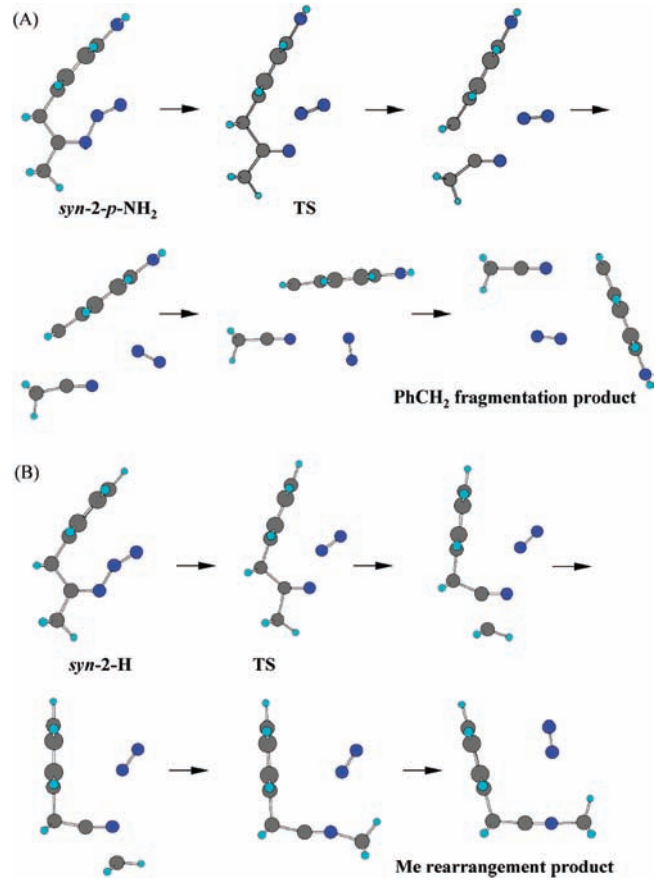

Figure 2. IRC snapshots from the TSs for (A) ***syn*-2-*p*-NH_2** and (B) ***syn*-2-H**.

(9) Grob, C. A.; Fischer, H. P.; Raudenbusch, W.; Zer'genyi, J. *Helv. Chim. Act* **1964**, *47*, 1003.
(10) Yamataka, H.; Sato, M.; Hasegawa, H.; Ammal, S. C. *Faraday Discuss.* **2010**, *145*, 327–340.
(11) Frisch, M. J. et al. *Gaussian 03, Revision C.02*; Gaussian, Inc.: Wallingford, CT, 2004.
(12) Herkstroeter, W. G. *J. Am. Chem. Soc.* **1973**, *95*, 8686. Hoffmann, H.-J.; Asano, T.; Cimiraglia, R.; Bonaccorsi, R. *Bull. Chem. Soc. Jpn.* **1993**, *66*, 130. Asano, T.; Furuta, H.; Hoffmann, H.-J.; Cimiraglia, R.; Tsuno, Y.; Fujio, M. *J. Org. Chem.* **1993**, *58*, 4418. Yamataka, H.; Ammal, S.; Asano, T.; Ohga, Y. *Bull. Chem. Soc. Jpn.* **2005**, *78*, 1851.

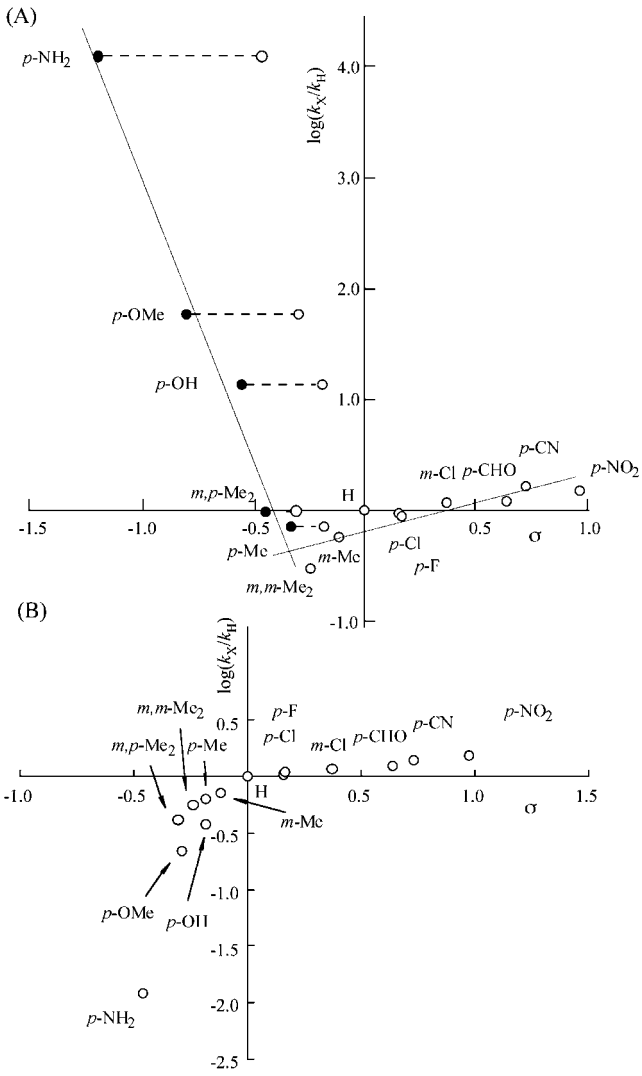

Figure 3. Hammett plots for the reactions of (A) ***syn*-2-X** and (B) ***anti*-2-X**. Relative reactivities at 298 K were calculated with the MP2/6-31G* enthalpies. Open circles are plots against the Hammett σ constants, and solid circles are against σ^+.

reaction mechanism is different for ***syn*-2-*p*-NH$_2$** and ***syn*-2-H**: $PhCH_2$ fragmentation for the former and Me rearrangement for the latter.

Relative activation enthalpies ($\Delta H^{\ddagger}$) in Table 2 were converted to $\log(k_X/k_H)$ at 298 K and were plotted against the Hammett σ constants in Figure 3A. Here, we used enthalpies, because the size of the entropy and hence the free energy depend much on low frequencies, which are less reliable than higher frequencies, especially for compounds with weak interactions such as TS. The use of free energy ($\Delta G^{\ddagger}$) gave similar correlations with more scattered points. The σ values were taken from gas-phase experiments.[13] The plots showed two separated correlation lines, one for $PhCH_2$ fragmentation (X = *p*-NH_2−*p*-Me), and the other for Me rearrangement (X = *m*,*m*-Me_2−*p*-NO_2). Since the $PhCH_2$ fragmentation generates substituted benzyl cations, the rates may be correlated better with σ^+ constants, which are shown as solid circles in Figure 3A.

(13) Huh, C.; Kang, C. H.; Lee, H. W.; Nakamura, H.; Mishima, M.; Tsuno, Y.; Yamataka, H. *Bull. Chem. Soc. Jpn.* **1999**, *72*, 1083. Mishima, M.; Mustanir; Fujio, M.; Tsuno, Y. *Bull. Chem. Soc. Jpn.* **1996**, *69*, 2009.

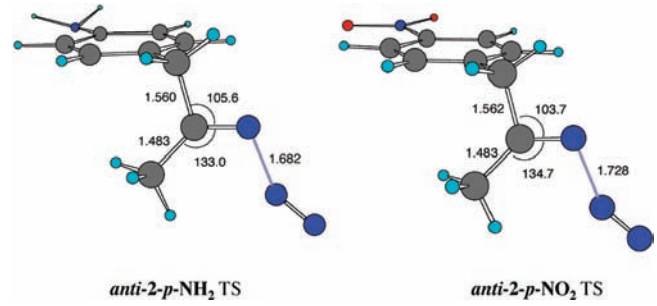

Figure 4. TS structures for ***anti*-2-X** (X = *p*-NH_2 and *p*-NO_2) at MP2/6-31G*. Atomic distances are in angstroms, and angles are in degrees.

Table 3. Calculated Activation Energies and Selected TS Geometrical Parameters at MP2/6-31G* for the Reactions of ***anti*-2-X**

X	activation energies[a]	reaction energies[b]	R_{Bn-C}[c]	R_{N-N2}[d]	θ_{Bn-C-N}[e]
p-NH_2	14.6 (13.0)	–32.3 (–57.7)	1.560	1.682	105.6
p-OMe	12.9 (11.5)	–28.1 (–53.7)	1.559	1.693	105.2
p-OH	12.6 (11.2)	–27.0 (–52.5)	1.560	1.696	105.0
m,*p*-Me_2	12.5 (11.3)	–47.0 (–62.2)	1.557	1.699	104.9
p-Me	12.3 (11.1)	–48.5 (–63.5)	1.558	1.701	104.7
m,*m*-Me_2	12.4 (11.3)	–47.9 (–62.8)	1.556	1.702	104.7
m-Me	12.2 (11.2)	–49.5 (–64.3)	1.557	1.705	104.6
H	12.0 (11.0)	–50.8 (–65.4)	1.559	1.707	104.5
p-F	12.0 (10.9)	–50.9 (–65.5)	1.561	1.708	104.4
p-Cl	12.0 (10.9)	–51.1 (–65.6)	1.561	1.710	104.3
m-Cl	11.9 (10.9)	–52.1 (–63.3)	1.559	1.719	104.1
p-CHO	11.9 (10.9)	–52.5 (–66.6)	1.560	1.719	104.1
p-CN	11.8 (10.8)	–53.7 (–62.5)	1.562	1.723	103.9
p-NO_2	11.8 (10.7)	–54.2 (–67.6)	1.562	1.728	103.7

[a] $\Delta H^{\ddagger}$ ($\Delta G^{\ddagger}$) in kcal/mol with respect to ***anti*-2-X**. [b] ΔH (ΔG) in kcal/mol with respect to ***anti*-2-X**. Reaction energies are for the fragmentation products for *p*-NH_2−*p*-OH and for $PhCH_2$-rearrangement products for *m*,*p*-Me_2−*p*-NO_2. [c] Distance between benzylic carbon and imino carbon in Å. [d] Distance between imino N and N_2 in Å. [e] Bn−C═N angle in deg.

The calculated V-shaped Hammett plots clearly indicate that the mechanism changes through path switching in concurrent and competitive reaction pathways. Such reaction mechanism with concurrent pathways should allow two TSs to be optimized for borderline substrates. This was indeed found for ***syn*-2-X** with X = *m*,*p*-Me_2, *p*-Me, *m*,*m*-Me_2, and *m*-Me (*vide infra*). The ρ value for the Me rearrangement was calculated to be 0.5, whereas the ρ^+ value for the $PhCH_2$ fragmentation was −5.0. These sizes of the ρ values are consistent with their respective electron demand of the reaction mechanisms. Finally, it should be mentioned that the *syn* $PhCH_2$ fragmentation is formally viewed as a concerted *syn* elimination and is a rare reaction, which becomes possible in the present system as a result of the intramolecular interaction between the Ar ring and the N_2 leaving group, which is positively charged at the TS.

Reaction of *anti*-2-X. Different from the reactions of ***syn*-2-X**, only one TS was found for each reaction of ***anti*-2-X**, even for borderline substrates. The calculated TS structures for ***anti*-2-X** with strongly electron-donating (***anti*-2-*p*-NH$_2$**) and electron-withdrawing (***anti*-2-*p*-NO$_2$**) substituents are illustrated in Figure 4, which shows that both TS structures look similar. The activation energies and selected geometrical parameters of the TSs are summarized in Table 3. The TS structure varies smoothly from a more product-like to a more reactant-like one when the substituent varies from electron-withdrawing NO_2 to electron-donating NH_2. The smooth TS variation itself is suggestive of the same reaction mechanism for all substituted substrates.

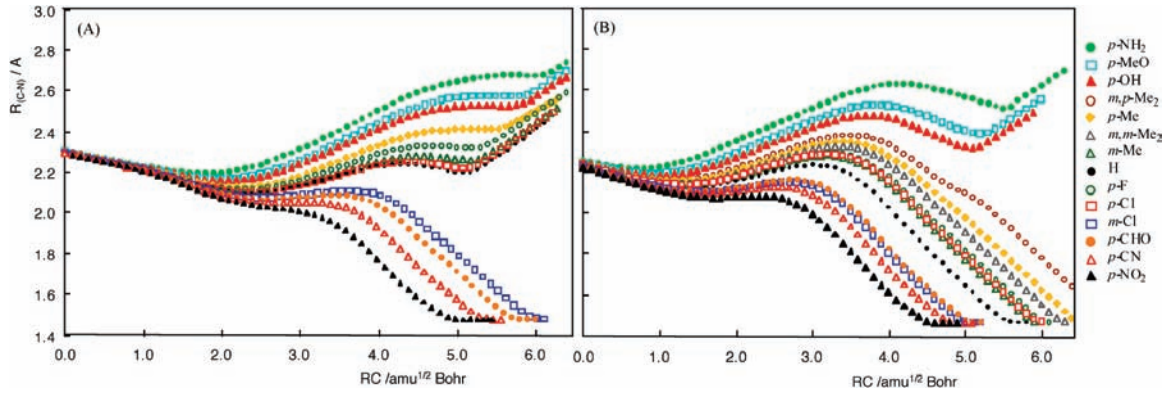

Figure 5. IRC pathways for the reactions of ***anti*-2-X** at (A) HF/6-31G* and (B) MP2/6-31G*.

Chart 1

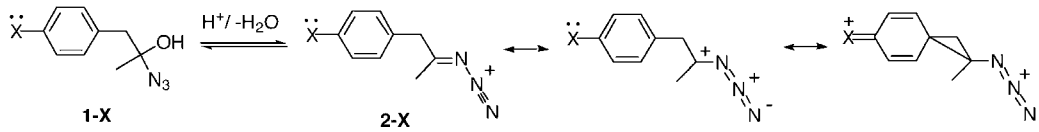

Although the TS structures thus appeared to suggest a common reaction mechanism for all substituted derivatives, IRC calculations revealed that the reaction mechanism varies depending on the electronic nature of the substituent, as shown in Figure 5. Here, the abscissa is the reaction coordinate and the ordinate is the atomic distance between the benzylic carbon and the inimo nitrogen, and only the IRC traces toward the products are shown. The C−N distance is shorter at the TS than at the reactant (e.g., 2.231 vs 2.362 Å, for X = H at MP2/6-31G*) and becomes as small as 1.4 Å in the rearrangement product, whereas it becomes larger than 2.5 Å on the way to the fragmentation product. It can be seen that the IRC for substrates with an electron-withdrawing substituent reached the rearrangement product state with a short C−N distance. On the other hand, the IRC for substrates with an electron-donating substituent led to the product with a long C−N distance. The two computational levels (HF and MP2) gave qualitatively the same results, in that the path switched from rearrangement to fragmentation when the substituent became more electron-donating. Overall, it is clear in Figure 5 that the IRC pathway varies with substituent, from clear rearrangement (X = *p*-NO_2, *p*-CN, *p*-CHO, and *m*-Cl) through borderline fragmentation-rearrangement (*p*-Cl, *m*-F, H, *m*-Me, *m*,*m*-Me_2, *p*-Me, and *m*,*p*-Me_2) to fragmentation (*p*-OH, *p*-MeO, and *p*-NH_2 at MP2) and that the product is either one of the two for each derivative, even for the borderline cases. As a result, despite the fact that the TS structure varies smoothly with substituent, the reaction product and the reaction mechanism on the PES exhibit a sharp change as a function of the substituent. The results of the IRC calculations are similar to those for the Beckmann reactions of 1-substituted-phenyl-2-propanone oximes.[10,14]

In the analogous Beckmann rearrangement/fragmentation reaction, the substituent effect on reactivity gave linear Hammett plots with a medium-sized ρ value of −7.1. However, the Hammett plots for the present Schmidt reaction gave puzzling results as shown in Figure 3B. Two points should be addressed. First, the ρ value is very small and even slightly positive despite the fact that the reaction may be characterized as a benzyl-cation generating reaction (fragmentation) or a Wagner−Meerwein-type 1,2-rearrangement reaction of benzyl group (rearrangement), both of which are normally considered to give negative ρ values. Second, the points of resonatively strong electron-donating groups deviate downward from the correlation line. It may be tempting to assume that the observed irregular plots arise from a mechanistic change from rearrangement to fragmentation with substituent in a competitive reaction scheme, since IRC suggested a change in the mechanism with substituent. However, this argument is inconsistent with the shape of the Hammett plot since a change in mechanism through a path switch should show concave upward plots as observed for the reactions of ***syn*-2-X** rather than convex plots as in Figure 3B. The observed strong downward deviation for ***anti*-2-*p*-NH_2** also disagrees with the interpretation.

The observed strong downward deviations for substrates with a *para* electron-donating substituent let us calculate substituent effects on the **1-X** (AH)/**2-X** (ID) equilibrium in order to examine the possibility that ID receives resonance stabilization by *para* electron-donating substituents through a phenonium ion type resonance structure as in Chart 1. The Hammett plots for the equilibrium (Figure S1 in Supporting Information) indeed gave a reasonably good correlation with a ρ value of −6.8, indicating that partial positive charge located on C in a resonance structure is delocalized into the aromatic ring. The Hammett plot for the **1-X**/**2-X** equilibrium for ***syn*-2-X** also gave a large ρ value of −9.1. The large substituent effect on the stability of ID of ***syn*-2-X** arises from the interaction between the aromatic ring and the N_2^+ leaving group in the ID form as mentioned above.

Thus, in order to gain information on the nature of the TS and the mechanism of the N_2 liberation step, it was better to examine the Hammett plots for the **1-X** → TS processes. Under the assumption that the substituent effect on the stability of **1-X** is small or negligible, the Hammett plots would give us information on the reaction mechanism of ***syn*-2-X** and ***anti*-2-X**.

The Hammett plots for the **1-X** → TS processes for ***syn*-2-X** and ***anti*-2-X** are illustrated in Figure 6. The plots for ***syn*-2-X**

(14) Ammal, S. C.; Yamataka, H. In *Recent Developments in Carbocation and Onium Ion Chemistry*; Laali, K. K. , Ed.; American Chemical Society: Washington, DC, 2007; p 364.

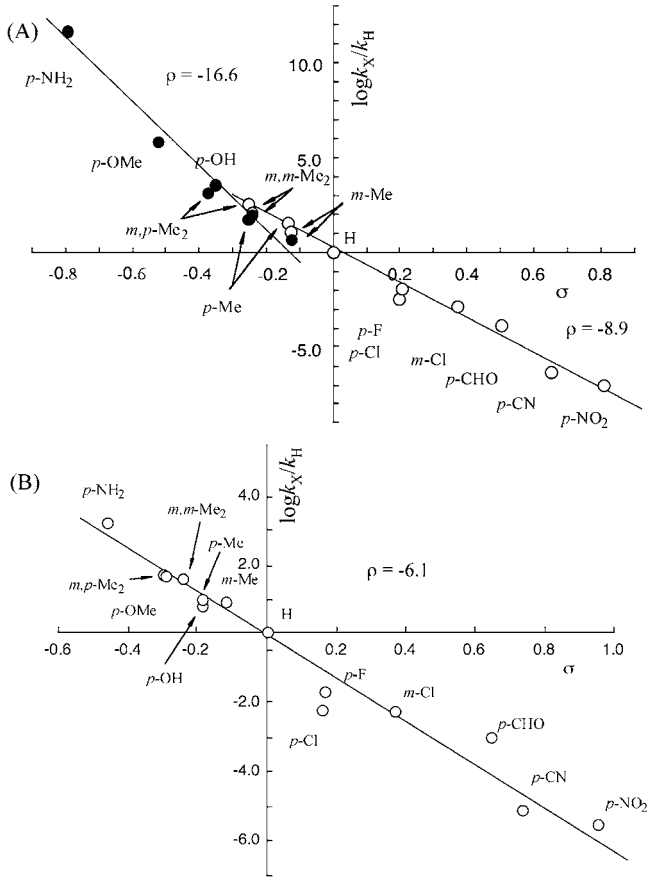

Figure 6. Hammett plot for the **1-X** → TS processes of (A) ***syn*-2-X** and (B) ***anti*-2-X**. Relative reactivities at 298 K were calculated with the MP2/6-31G* enthalpies. In Figure 6A, open circles are plots against the Hammett σ° constants for Me rearrangement reactions, and solid circles are against apparent σ constants with $r = 0.6$ in the Yukawa−Tsuno equation for benzyl fragmentation reactions. Open circles in Figure 6B are plots against Hammett σ constants for the reaction of ***anti*-2-X**.

in Figure 6A shows two independent lines, one for benzyl cation fragmentation (solid circles) and the other for Me rearrangement (open circles). The ***syn*-2-X** species having electron-donating substituents gave a reasonably good correlation with $r = 0.6$ in the Yukawa−Tsuno equation (eq 3),[15] showing significant carbocationic character at the TS, consistent with the fragmentation process. The ***syn*-2-X** species with weakly electron-donating or electron-withdrawing substituents showed good linear correlation against the σ° constants, consistent with negligible resonance effects at the Me rearrangement TSs. An important point in Figure 6A is that two TSs were obtained for each of the borderline substrates (X = *m*,*p*-Me_2, *p*-Me, *m*,*m*-Me_2, and *m*-Me). For X = *m*,*p*-Me_2 and *p*-Me, the $PhCH_2$-fragmentation TSs are more stable, whereas Me-rearrangement TSs are more stable for X = *m*,*m*-Me_2 and *m*-Me. The overall concave upward plots are consistent with the concurrent and competitive reaction pathways for ***syn*-2-X**.

$$\log(k/k_0) = \rho\{\sigma^\circ + r(\sigma^+ - \sigma^\circ)\} \qquad (3)$$

In contrast to the reactions of ***syn*-2-X**, the reactions of ***anti*-2-X** gave reasonably good linear Hammett plots against the standard Hammett σ constants. The observed negative ρ value of medium size (−6.1) is similar in magnitude to that (−7.1) reported previously for the Beckmann rearrangement/fragmentation reaction of 3-X-substituted phenyl-2-butanone oximes.[10] The results suggest that both the Schmidt and Beckmann reactions proceed through TSs with similar characteristics, and that the Schmidt reaction may also exhibit path bifurcation as was observed for the Beckmann reaction.

It is important to point out that the Hammett plot in Figure 6B is linear, despite the fact that ***anti*-2-X** with electron-donating substituents lead to fragmentation products, whereas ***anti*-2-X** with electron-withdrawing substituents yield rearrangement products on the PES. Thus, the Hammett plot failed to detect the change in mechanism with substituent. Finally, it is worth noticing that the ρ value for the ***anti*-2-X** reactions is more than two times smaller than the ρ value for the fragmentation pathway of ***syn*-2-X**, which indicates that the nature of the TSs for the reactions of ***anti*-2-X** is different from that of the *syn*-fragmentation reactions, although the reactions of ***anti*-2-X** with electron-donating substituents gave fragmentation products.

Rate−Equilibrium Correlation. Correlation plots between the activation and reaction energies are often informative in elucidating the nature of the TS. In the present reactions, both *syn* and *anti* substrates gave either of the two products depending on the substituent. The activation and reaction enthalpies with respect to **1-X** were used to construct the correlation plots, since as was shown with Hammett plots, the stabilities of ID ions receive large substituent effects, which may mask the nature of the substituent effects on the TSs. The plots of $\delta\Delta H^\ddagger$ versus $\delta\Delta H$ for the reaction of **1-X** → ***syn*-TS** → benzyl-fragmentation products gave a good straight line for the three electron-donating substituents (*p*-NH_2, *p*-MeO, and *p*-OH), whereas points for other substituents deviated upward from the correlation line with some scattering (Figure 7A). The results indicated that the three substrates go though benzyl-fragmentation TS, and other substrates go through TSs that are more stable than hypothetical benzyl-fragmentation TSs. The scattering was observed for open circles in Figure 7A because the stability of substituted benzyl cations is not a good measure of the stability of Me-rearrangement TSs. Similarly, correlation plots of $\delta\Delta H^\ddagger$ versus $\delta\Delta H$ for Me-rearrangement products gave reasonable a good straight line for electron-withdrawing substituents, and the points for electron-donating substituents (*p*-NH_2, *p*-MeO, and *p* -OH) deviated upward from the correlation line (Figure S2 in Supporting Information). These correlation plots are consistent with the mechanism with concurrent and competitive reaction pathways as described above.

The rate-equilibrium correlation ($\delta\Delta H^\ddagger$ vs $\delta\Delta H$) for **1-X** → ***anti*-TS** → **3-X** showed a completely different picture; the plots gave an excellent linear correlation ($R^2 = 0.9996$) for all substituents with a slope of 1.00 (Figure 7B). This clearly indicated that the TSs for all substituents have characters of benzyl-rearrangement TS, despite the fact that IRCs from the TSs lead to the fragmentation products for three substrates with X = *p*-NH_2, *p*-MeO, and *p*-OH and to the rearrangement products for other substrates. Thus, the TSs do not have enough information about what type of products they will give. The identity of the product is determined at a post-TS region on the reaction coordinate. The observed large slope of near unity is not an abnormal one since the plot is not an ordinary Brønsted-type plot in the sense that the TS is not midway from the reactant to the product state with respect to the nature of the migrating benzyl group where perturbation is given. The slope is large because the TS receives considerable magnitude of substituent

(15) Yukawa, Y.; Tsuno, Y. *Bull. Chem. Soc. Jpn.* **1959**, *32*, 971. Yukawa, Y.; Tsuno, Y.; Sawada, M. *Bull. Chem. Soc. Jpn.* **1966**, *39*, 2274.

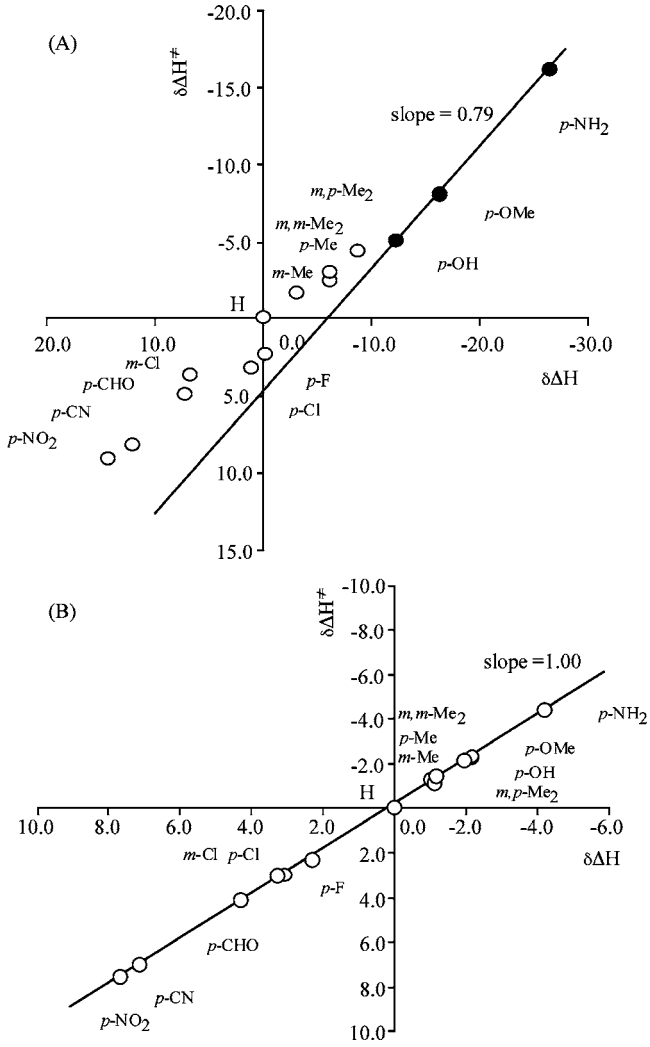

Figure 7. Rate−equilibrium correlation between the activation and reaction energies, relative to the parent compounds (X = H), for the reactions of (A) **1-X** → ***syn*-TS** → **4-X** and (B) **1-X** → ***anti*-TS** → **3-X**. Solid circles in Figure 7A are for substrates that lead to benzyl fragmentation products by IRC, and open circles are for those that give Me-rearrangement products.

effects as evidenced by the ρ value (−6.1) of the Hammett plot in Figure 6B, whereas the substituted benzene ring is two or three bonds apart from the cationic center in the resonance structures of the benzyl rearrangement product.

Trajectory Calculations. MO calculations revealed that substituent effects gave a linear Hammett plot for the Schmidt reaction of ***anti*-2-X**, whereas IRC calculations showed that the TSs led to different products depending on the substituent. Thus, the reaction product, and hence the reaction mechanism, does not affect character of the TSs.

According to traditional interpretation of chemical reactions, the reaction rate and hence the product selectivity are governed by the activation energy and its variation. It has been increasingly recognized that in some mechanistic borderline reactions, post-TS dynamics may not always follow IRCs and that the argument based on the TS and the PES fails.[16] The dynamics effect appears in different ways,[16e] such as nonstatistical barrier recrossing,[17] nonstatistical product distribution,[18] shallow minimum skip on IRC,[19] non-IRC path,[20,21] path bifurcation,[22,23] and even flying over low-lying TS.[24] All these results suggested that the mechanism of these reactions could not be defined by the traditional TS theory.

We have recently reported that in the Beckmann rearrangement/fragmentation reactions, the reaction pathway did not follow the minimum energy path (MEP) on the PES, and the reaction pathways bifurcated after the TS.[10] As a result, the two types of products were formed through a common TS, which means that the TS has little relevance to the product selectivity. Although the level of computation was rather low at HF/6-31G*, the results suggested that path bifurcation could occur in a common textbook reaction. It is inevitably necessary to examine with a better computational theory whether such path bifurcation occurs in another common reaction. Thus, we have carried out MD simulations on the Schmidt rearrangement/fragmentation reaction at both HF and MP2 levels of theory.

Direct MD simulations were carried out both at HF/6-31G* and MP2/6-31G* starting at respective TSs of ***anti*-2-X** with selected substituents in order to see how the mechanism changes with substituent. A total of 980 trajectory runs at HF/6-31G* for X = *p*-MeO, *p*-Me, H, *m*-Cl, *p*-CN, and *p*-NO_2 and 85 runs at MP2/6-31G* for X = *p*-MeO, H, and *p*-NO_2 were obtained. Typical examples of the trajectories are illustrated in Figure 8, in which the abscissa is the N−N atomic distance and the ordinate is the atomic distance between the benzylic carbon and the imino nitrogen.

In Figure 8, a trajectory that goes to the region of a C−N distance shorter than 1.6 Å is arbitrarily assigned as a rearrangement trajectory (type R), whereas a trajectory that leads to the product region with a long C−N distance is called a

(16) (a) Carpenter, B. K. *Acc. Chem. Res.* **1992**, *25*, 520. (b) Carpenter, B. K. *Angew. Chem., Int. Ed.* **1998**, *37*, 3340. (c) Carpenter, B. K. *J. Phys. Org. Chem.* **2003**, *16*, 858. (d) Ess, D. H.; Wheeler, S. E.; Iafe, R. G.; Xu, L.; Çelebi-Ölçüm, N.; Houk, K. N. *Angew. Chem. Int. Ed* **2008**, *47*, 7592. (e) Yamataka, H. In *Advances in Physical Organic Chemistry*; Richard, J. P., Ed.; Academic Press: New York, 2010; Vol. 44, in press.
(17) Sun, L.; Hase, W. L.; Song, K. *J. Am. Chem. Soc.* **2001**, *123*, 5753. Cheon, S.; Song, K.; Hase, W. L. *THEOCHEM* **2006**, *771*, 27.
(18) Carpenter, B. K. *J. Am. Chem. Soc.* **1995**, *117*, 6336. Doubleday, C.; Li, G.; Hase, W. L. *Phys. Chem. Chem. Phys.* **2002**, *4*, 304. Doubleday, C.; Suhrada, C. P.; Houk, K. N. *J. Am. Chem. Soc.* **2006**, *128*, 90. Litovitz, A. E.; Keresztes, I.; Carpenter, B. K. *J. Am. Chem. Soc.* **2008**, *130*, 12085.
(19) Debbert, S. L.; Carpenter, B. K.; Hrovat, D. A.; Borden, W. T. *J. Am. Chem. Soc.* **2002**, *124*, 7896. Nummela, J. A.; Carpenter, B. K. *J. Am. Chem. Soc.* **2002**, *124*, 8512. Sun, L.; Song, K.; Hase, W. L. *Science* **2002**, *296*, 875. Anand, S.; Schlegel, H. B. *Phys. Chem. Chem. Phys.* **2004**, *6*, 5166. Hamaguchi, M.; Nakaishi, M.; Nagai, T.; Nakamura, T.; Abe, M. *J. Am. Chem. Soc.* **2007**, *129*, 12981.
(20) Ammal, S. C.; Yamataka, H.; Aida, M.; Dupuis, M. *Science* **2003**, *299*, 1555. Townsend, D.; Lahankar, S. A.; Lee, S. K.; Chambreau, S. D.; Suits, A. G.; Zhang, X.; Rheinecker, J.; Harding, L. B.; Bowman, J. M. *Science* **2004**, *306*, 1158. Pomerantz, A.; Camden, J. P.; Chioiu, A. S.; Ausfelder, F.; Chawia, N.; Hase, W. L.; Zare, R. N. *J. Am. Chem. Soc.* **2005**, *127*, 16368.
(21) Bekele, T.; Christian, C. F.; Lipton, M. A.; Singleton, D. A. *J. Am. Chem. Soc.* **2005**, *127*, 9216.
(22) Singleton, D. A.; Hang, C.; Syzmanski, M. J.; Greenwald, E. *J. Am. Chem. Soc.* **2003**, *125*, 1176. Ammal, S.; Yamataka, H. *Eur. J. Org. Chem.* **2006**, 4327. Leach, A. G.; Houk, K. N.; Foote, C. S. *J. Org. Chem.* **2008**, *73*, 8511. Kelly, K. K.; Hirschi, J. S.; Singleton, D. A. *J. Am. Chem. Soc.* **2009**, *131*, 8382.
(23) Yamataka, H.; Aida, M.; Dupuis, M. *Chem. Phys. Lett.* **1999**, *300*, 583. Bakken, V.; Danovich, D.; Shaik, S.; Schlegel, H. B. *J. Am. Chem. Soc.* **2001**, *123*, 130. Taketsugu, T.; Kumeda, Y. *J. Chem. Phys.* **2001**, *114*, 6973. Yamataka, H.; Aida, M.; Dupuis, M. *J. Phys. Org. Chem.* **2003**, *16*, 475. Li, J.; Li, X.; Shaik, S.; Schlegel, H. B. *J. Phys. Chem. A* **2004**, *108*, 8526. Ussing, B. R.; Hang, C.; Singleton, D. A. *J. Am. Chem. Soc.* **2006**, *128*, 7594. Çelebi-Ölçüm, N.; Ess, D, H,; Aviyente, V.; Houk, K. N. *J. Org. Chem.* **2008**, *73*, 7472.
(24) Oyola, Y.; Singleton, D. A. *J. Am. Chem. Soc.* **2009**, *131*, 3130.

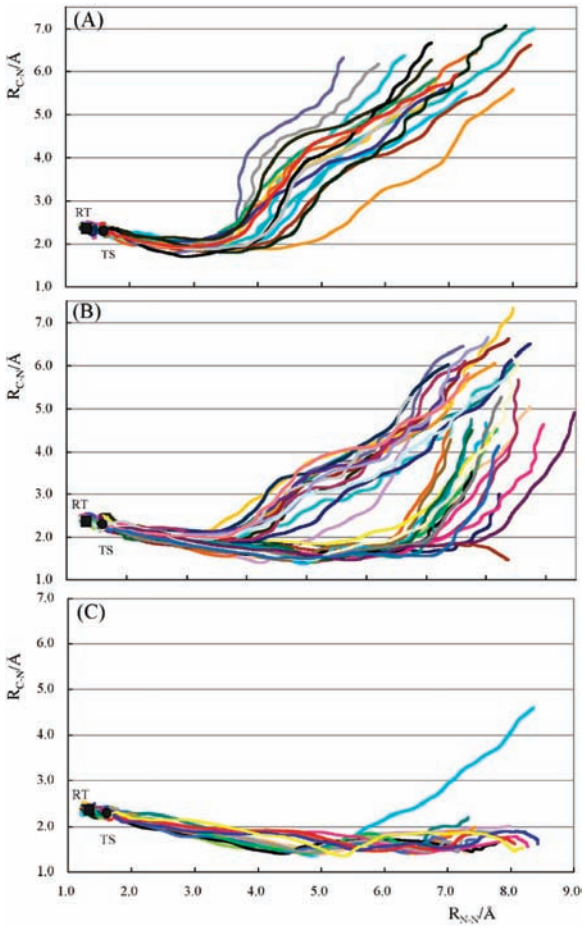

Figure 8. Two-dimensional plots of MD trajectories obtained by Gaussian03 at HF/6-31G*: (A) ***anti*-2-*p*-MeO**, (B) ***anti*-2-H**, and (C) ***anti*-2-*p*-NO_2**. The abscissa is the N···N distance and the ordinate is the $ArCH_2$···N distance in angstroms.

fragmentation trajectory (type F). There are some trajectories that initially go to the rearrangement region and then lead to the fragmentation product, and they are counted as type R.

The results for ***anti*-2-*p*-MeO** in Figure 8A clearly indicate that all trajectories directly lead to the fragmentation region (type F). In Figure 8C are shown the trajectories for ***anti*-2-*p*-NO_2**, all of which are type R. Thus, trajectory calculations for these two substrates gave results that agreed with the IRC calculations shown in Figure 5A. In contrast, simulations with one of the borderline substrates (***anti*-2-H**) gave both type F and R trajectories as illustrated in Figure 8B.

Many of the trajectories that initially led to the rearrangement product region for ***anti*-2-H** ended up in the fragmentation product region in a longer time scale. This occurred because there was no solvent that trapped the cationic intermediate in the gas-phase trajectory calculations and also because trajectories that reached the product region had enough internal energy to overcome the barrier separating the two product states. In the present study, we focus on the initial or kinetic controlled branching ratios of the trajectories. Table 4 summarizes the results of trajectory calculations for six substituted derivatives. Although the reason is unknown why the number of productive runs toward the product regions is not large compared to those toward the reactant region, we have enough trajectories to qualitatively see the effect of substituent on the F/R product ratio. It is clear that both HF and MP2 showed qualitatively the same trends. Substrates with an electron-withdrawing substituent led to the rearrangement region exclusively, whereas those with an electron-donating substituent gave predominantly the fragmentation products. For the borderline substrates, trajectories from their respective TS gave both fragmentation and rearrangement products directly. The observed similar trends indicate that the occurrence of path bifurcation is not an artifact due to the low level of computation.

Table 4. Summary of the Trajectory Calculations for ***anti*-2-X**

method	X	n^a	R^b	F^c	R%^{d}	IRC^e
HF/6-31G*	*p*-MeO	100	0	16	0	F
	p-Me	270	10	23	30	F
	H	180	17	17	50	F
	m-Cl	150	21	12	64	R
	p-CN	170	23	9	72	R
	p-NO_2	110	16	0	100	R
MP2/6-31G*	*p*-MeO	25	2	9	18	F
	H	50	16	2	89	R
	p-NO_2	10	10	0	100	R

[a] Number of trajectories. [b] Number of trajectories that initially lead to the rearrangement region. [c] Number of trajectories that lead to the fragmentation region. [d] % Rearrangement $= 100(R/(R + F))$. [e] IRC leading to rearrangement (R) or fragmentation (F) product.

Path Bifurcation. The fact that the trajectories starting from a TS lead to two products indicates that the reaction path bifurcates dynamically on the way from the TS to the products, despite the fact that the IRC path on the PES is connected to either one of the two products for the substrate. Such a path bifurcation phenomenon clearly violates the TS-based reaction theory and thus suggests that a TS of a given character may have only limited significance with respect to the actual mechanism.

Two types of path bifurcation have been observed in previous direct-MD simulations in the literature.[22,23] One is related to a symmetrical PES schematically shown in Figure 9A, in which the MEP from the TS that separates the reactant and product regions leads through a valley-ridge inflection (VRI) point to another TS separating two symmetrical products.[25] Trajectories starting from the first TS proceed toward the second TS and bifurcate before reaching the second TS to give two products in statistically equal amounts. When a small perturbation, such as an isotope or a remote substituent, is introduced, the two products would be formed in different amounts.[22] The product ratio is controlled by the way trajectories adopt the course on the way from the first TS to the second TS. In the second and less-known type, MEP from a TS leads to one product that is separated by the second TS from another product located nearby on the PES (Figure 9B).[23] Bifurcation on such asymmetrical PES may occur when trajectories move off the MEP dynamically before reaching the first product region and get over a barrier toward the second product region.

The present Schmidt rearrangement/fragmentation falls in the second category. Thus, trajectories from the TSs for ***anti*-2-*p*-MeO** led mostly to the fragmentation product region, whereas those for ***anti*-2-*p*-NO_2** went to the rearrangement product region. In these cases, the trajectories basically followed the IRCs. For borderline substrates, however, trajectories starting from the respective TS bifurcated and led to two product regions. In these cases, more F-type trajectories were detected for ***anti*-2-X** with a more electron-donating substituent. The present observations are explained by the shift of the barrier separating

(25) Quapp, W.; Hirsch, M.; Heidrich, D. *Theor. Chem. Acc.* **2004**, *112*, 40, and references therein.

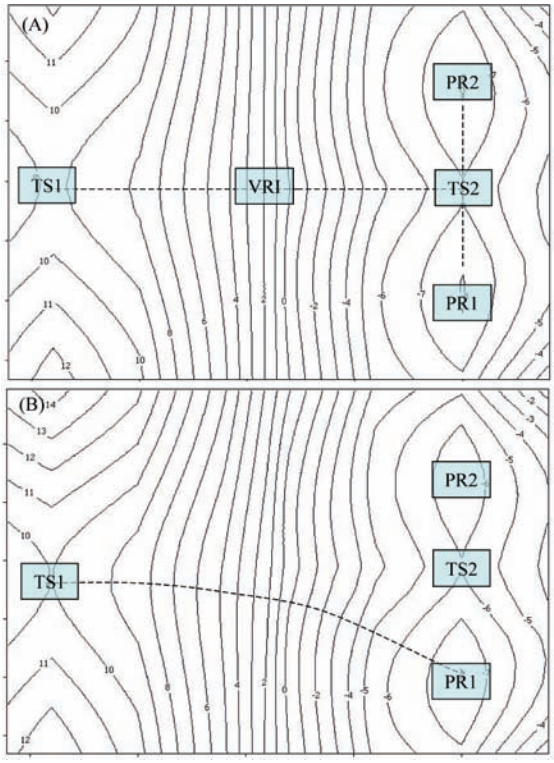

Figure 9. Schematic illustration of (A) symmetric and (B) asymmetric two-dimensional PESs. Axes are appropriate degrees of internal freedom of the reacting system.

the two product regions with substituent. Here the two product regions (R and F) are separated by the TS for the $CH_3CN\cdots CH_2Ar$ bond formation, and IRC coming down from the first TS leads to either of the two product states depending on the relative stability of the R and F regions. MD trajectory takes a path similar to the IRC, but since trajectory has finite kinetic energy, it may take variable paths depending on the initial conditions. As a result, trajectories starting from the first TS may give both R and F products, the ratio of which depends on the location of the second TS separating the R and F regions. The present result that more F-type trajectories were obtained for ***anti*-2-X** with a more electron-donating substituent is explained by the shift of the second TS with substituent. Since an electron-donating substituent makes the fragmentation product more stable, the TS should move toward the rearrangement side, and then more trajectories would go to the fragmentation side. The shift of the TS is consistent with the Leffler−Hammond principle[26] and the Thornton rule[27] and was indeed confirmed by the position of the calculated TS as summarized in Table 5. Here, since the TS for the simple $CH_3CN\cdots CH_2Ar$ bond dissociation is difficult to locate in the gas phase, the TS at the MP2 level could be located only for X = *p*-MeO, whose bond dissociation was not too endothermic. Nevertheless, the calculations at the HF level gave a series of TSs, which clearly indicated that the position of the TS shifts to the rearrangement product side for a more electron-donating substituent. The fact that fragmentation route was favored with HF than with MP2 both in IRC and MD simulation is consistent with the reaction energy differences for the two computational methods listed in Table 5.

Table 5. Activation and Reaction Energies and $CH_3CN\cdots CH_2Ar$ Distance at the TS for the Bond Dissociation Process of CH_3CN-CH_2Ar Cation Calculated at HF/6-31G*[a]

X	ΔH^b	ΔG^b	$\Delta H^{\ddagger}$	$\Delta G^{\ddagger}$	$R_{N-C}{}^{\ddagger}$
p-OMe	5.0 (16.7)	–5.4 (6.6)	6.1 (9.4)	5.4 (8.4)	1.907 (2.008)
p-Me	13.5	3.4	8.4	7.7	1.980
H	18.8 (30.8)	8.7(20.8)	10.0	9.1	2.033
p-CN	26.3	16.0	13.1	12.0	2.142
p-NO_2	30.5 (37.5)	19.8 (26.7)	15.0	13.2	2.276

[a] Energies are with respect to the rearrangement product in kcal/mol and distances are in Å. Numbers in parentheses are those at MP2/6-31G*. [b] Energies of the fragmentation product states are for separated species ($ArCH_2^+ + CH_3CN$) rather than product complexes.

It is important to point out here that the product ratio is thus governed by the electronic nature of substituents in a manner consistent with the traditional electronic theory. As a result, the dynamically controlled substituent effects on the product distribution could readily be reconciled with the traditional reaction theory, which implies that such path bifurcation phenomenon would easily be overlooked by experiment, unless critical and well-planned experiments were made.

Concluding Remarks

The present MO calculations on the Schmidt reaction led to several important conclusions. First, the barrier of *syn*−*anti* isomerization of iminodiazonium ion (**2-X**) is much larger than that of the Schmidt reaction itself, and ***syn*-2** is more stable than ***anti*-2** for all **2-X** at MP2. Second, two reaction channels exist for ***syn*-2**, *syn*-benzyl fragmentation and *anti*-Me rearrangement, and ***syn*-2-X** with an electron-donating X favors benzyl fragmentation, whereas those with an electron-withdrawing substituent go through the Me-rearrangement channel. For borderline substrates two TSs were obtained with similar stabilities. Substituent effect analyses of the reaction of ***syn*-2-X** gave concave-upward plots typical for a concurrent reaction mechanism. On the other hand, the reaction of ***anti*-2-X** proceeds via a single TS and gave linear Hammett plots, indicative of single reaction mechanism for all ***anti*-2-X**. By contrast, IRC calculations revealed that the TS either led to an *anti*-benzyl rearrangement or an *anti*-benzyl fragmentation product depending on the substituent. Introduction of an electron-donating substituent into the phenyl ring changes the mechanism from rearrangement for X = *p*-NO_2, *p*-CN, *p*-CHO, *m*-Cl, *p*-Cl, *p*-F, H, *m*-Me, *m*,*m*-Me_2, and *m*,*p*-Me_2 to fragmentation for X = *p*-OH, *p*-MeO, and *p*-NH_2 (at MP2). Thus, the change of the product and the reaction mechanism could not be detected by the Hammett plots. It is implied that Hammett plots and analyses of TS structures may lead to incorrect conclusion of the reaction mechanism.

Ab initio dynamics simulations for ***anti*-2-X** were found to follow the IRC path for X = *p*-NO_2, giving the rearrangement product, and almost so for X = *p*-MeO, giving the fragmentation products. However, in borderline cases where X is less donating than *p*-MeO and less withdrawing than *p*-NO_2, the trajectories did not perfectly follow MEP on PES but instead gave both rearrangement and fragmentation products directly from the single TS. It was concluded that a reactivity-selectivity argument based on the traditional TS theory may not always be applicable even to a well-known textbook organic reaction. It should also be noted that the dynamically determined product ratio is governed by the electronic nature of substituents in a manner

(26) Leffler, J. E. *Science* **1953**, *117*, 340. Hammond, G. S. *J. Am. Chem. Soc.* **1955**, *77*, 334.

(27) Thornton, E. R. *J. Am. Chem. Soc.* **1976**, *89*, 2915.

consistent with traditional electronic theory. Thus, the dynamic substituent effects on the product distribution are readily reconciled with traditional reaction theory, which means that such a path bifurcation phenomenon would not easily be detected by experiment, unless critical examinations of experimental results were made. Measurements of substituent effects and KIEs, which are common means to detect variation of TS structures and reaction mechanisms, should be planned with care, since these experimental methods applied to rate processes do not afford information of possible path bifurcation occurring after the TS.

Finally, it is worth analyzing why path bifurcation is observed for the reaction of ***anti*-2-X**, or in what case in general we could expect path bifurcation. In the present case, the reactions of ***syn*-2-X** proceed via the mechanism with concurrent pathways, whereas the reactions of ***anti*-2-X** proceed via bifurcation after a TS. The rearrangement and fragmentation TSs for ***syn*-2-X** involve separate reaction coordinates, C-Me bond breaking and C-CH_2Ph bond breaking, and hence ***syn*-2-X** reacts via the competitive reaction scheme. On the other hand, the rearrangement and fragmentation TSs for ***anti*-2-X** share the same reaction coordinates, C-CH_2Ph bond breaking. Under the circumstances, two products may form via a single TS, and in the present case more fragmentation is observed for ***anti*-2-X** with a more electron-donating substituent.

Acknowledgment. The study was in part supported by the SFR aid by Rikkyo University.

Supporting Information Available: Complete ref 11. Optimized structures, energies, and imaginary frequencies, when available, for all species discussed in this paper. Hammett plots for the equilibrium between AH and ID, and correlation between the activation and reaction energies for the reactions of **1-X** → ***syn*-TS** → **3-X**. This material is available free of charge via the Internet at http://pubs.acs.org.

JA908899U